Multiple phase and dielectric transitions on a novel multi-sensitive [TPrA][M(dca)₃] (M: Fe²⁺, Co²⁺ and Ni²⁺) hybrid inorganic–organic perovskite family†

J. M. Bermúdez-García,*[a] M. Sánchez-Andújar,[a] S. Yáñez-Vilar,[ab] S. Castro-García,[a] R. Artiaga,[c] J. López-Beceiro,[c] L. Botana,[d] A. Alegría[de] and M. A. Señarís-Rodríguez*[a]

The hybrid inorganic–organic [TPrA][M(dca)₃] (M: Fe²⁺, Co²⁺ and Ni²⁺) compounds, where TPrA is the tetrapropylammonium cation and dca is the dicyanamide anion, are unique multi-sensitive compounds that display multiple phases and dielectric transitions. These materials exhibit up to three first-order structural transitions (between the polymorphs I, Ia, Ib and II) associated with the same number of dielectric transitions in the temperature range of 210–360 K. The mechanisms responsible for these dielectric responses are found to be novel within the hybrid perovskites, involving ionic displacements of the A-site cations (TPrA) and order/disorder processes of the X anions (dca). In addition, the phase transitions and dielectric transition temperatures can be tuned by applying external hydrostatic pressure or by inducing internal pressure by modifying the tolerance factor through ionic substitution in the B-sites. This multi-sensitive response towards temperature, external and internal pressure opens up promising technological applications for this family of materials, such as dielectric transductors or multistimuli-sensors, whose response can be modulated in a wide range of temperatures and pressures.

1. Introduction

Perovskites, and the phase transitions they can experience as a function of temperature, pressure, *etc.*, have been at the center of a vast amount of research in solid state and material science over the last decades[1] in view of their huge scientific and technological interest. In that context, early studies on conventional inorganic perovskites, ABX₃ (A: lanthanides, alkaline-earth metals or similar cations, B: transition metal cations and X: oxide, sulphide or halide anions, *etc.*), specially mixed oxides,

highlighted the exceptional functional and even multi-functional properties. This is the case, among others, of the very well-known and widely used ferroelectric BaTiO₃, the piezoelectric Pb(Zr₁₋ₓTiₓ)O₃ (PZTs),[2] the high temperature superconductor YBa₂Cu₃O₇₋δ,[3] the colossal magnetoresistive La₁₋ₓCaₓMnO₃,[4] the mixed ionic–electronic conductors La₁₋ₓSrₓCoO₃₋δ,[1a] or more recently, the multiferroic BiFeO₃.[5]

Interestingly, in the last few years, significant efforts have been devoted to the development of new members of the versatile family of the so-called perovskite-like hybrid inorganic–organic materials,[6] where the A- and/or X-site inorganic moieties of the conventional perovskites have been replaced by organic building blocks. Some of these materials, despite their recentness, have already revealed very remarkable functional properties. This is the case of the (MA)PbI₃ (MA = methylammonium cation),[7] which has revealed unprecedented photoconductivity; or the noteworthy [AmineH][M(X)₃] families (AmineH = midsized protonated amines in the A-site position of the perovskite, M = different divalent transition metal cations in the B-site, X = different bidentate-bridge ligands in the X-site position, such as N₃⁻, CN⁻ or HCOO⁻), which exhibit cooperative magnetic, electric or elastic order, even multiferroicity, associated in many cases to very interesting thermally-induced phase transitions.[8–17] Very remarkably, magnetoelectric coupling has been recently reported experimentally in the paramagnetic state of [(CH₃)₂NH₂][Fe(HCOO)₃],[16]

[a] *QuiMolMat Group, Department of Fundamental Chemistry, Faculty of Science and CICA, University of A Coruña, Campus A Coruña, 15071 A Coruña, Spain. E-mail: j.bermudez@udc.es, m.senaris.rodriguez@udc.es*

[b] *Department of Applied Physics, University of Santiago de Compostela, 15782 Santiago de Compostela, Spain*

[c] *Department of Industrial Engineering II, University of A Coruña, Campus Ferrol, 15403 Ferrol, Spain*

[d] *Material Physical Center, CSIC-UPV/EHU, P. Manuel de Lardizabal 5, 20018 Donostia-San Sebastian, Spain*

[e] *Material Physical Department, University of the Basque Country, PO Box 1072, 20008 Donostia-San Sebastian, Spain*

† Electronic supplementary information (ESI) available: Powder XRD patterns, details of the crystal structure, graphics of the variation of the phase transition temperatures with the tolerance factor and external pressure, table of enthalpy and entropy values obtained by DSC, summary of crystallographic data and CIF (CSD number: 431135–431145). See DOI: 10.1039/c6tc00723f

This journal is © The Royal Society of Chemistry 2016

J. Mater. Chem. C, 2016, 4, 4889–4898 | 4889

and ferroelectricity induced by magnetic order has been demonstrated in $[CH_3NH_3][Co(HCOO)_3]$,[17] opening the large, flexible, multifunctional and designable family of hybrid perovskites to magnetically induced multiferroic behaviour.

Another related, but so far much less explored, family of potentially interesting compounds is that of metal-dicyanamides with the formula $[AmineH][M(dca)_3]$ and has perovskite-like structure. In these compounds, the dicyanamide anions, $[N(CN)_2]^-$ (dca), bridge the transition metal cations (up to now, M: Mn^{2+} ref. 18 and 19 and Ni^{2+} ref. 18) in a $\mu_{1,5}$-dca end-to-end mode, forming a 3D framework. Meanwhile, the protonated amines (so far tetrapropylammonium, $[(CH_3CH_2CH_2)_4N]^+$ or TPrA) are located in the resulting pseudo-cubooctahedral cavities.[18]

In our previous work,[19] we have revisited the Mn compound $[TPrA][M(dca)_3]$, finding a structural transition at 330 K, and studied the influence of external pressure on the structural and dielectric properties of this compound. Interestingly enough, we found that this material had a new type-I multiferroicity that was very sensitive to temperature and external pressure.

In the present work, we enlarge the family of $[TPrA][M(dca)_3]$ perovskites with two new members (M: Fe^{2+} and Co^{2+}) that we describe for the first time; and we shed light on the unexplored structural features of the Ni compound, for which two structural transitions had been previously reported at 160 K and 210 K,[18] and we present two new additional polymorphs.

We also explore the dielectric properties of these materials and present a systematic and careful study of the effect of external and internal pressure on the structural transitions and dielectric responses of these three $[TPrA][M(dca)_3]$ (M: Fe^{2+}, Co^{2+} and Ni^{2+}) compounds.

Very interestingly, and as we will show below, we have found that these Fe, Co, and Ni compounds display multiple phase transitions responsible for multiple dielectric transitions that are both very sensitive to temperature as well as to external and internal pressure.

2. Experimental

2.1 Synthesis

$[TPrA][M(dca)_3]$ (M: Fe^{2+}, Co^{2+} and Ni^{2+}) materials were prepared from commercially available $FeCl_2·4H_2O$ (98%, Sigma-Aldrich), $Co(NO_3)_2·6H_2O$ (98%, Sigma-Aldrich), $Ni(NO_3)_2·6H_2O$ ($\geq 98.5\%$, Sigma-Aldrich), (TPrA)Br (98%, Aldrich), Na(dca) (96%, Aldrich) and absolute ethanol (Panreac), which were used as purchased without further purification. A reagent amount of deionised water was also used in the synthesis.

The synthetic route used here is an adaptation of the previously reported method for the preparation of the $[TPrA][M(dca)_3]$ compounds (M: Mn^{2+} and Ni^{2+}),[18] where synthesis of the metal dicyanamide frameworks were templated by alkylammonium cations and accomplished through a mild solution chemistry method at room temperature.

In a typical experiment, 10 ml of an aqueous solution containing 2 mmol of $FeCl_2·4H_2O$ or $M(NO_3)_2·6H_2O$ (M: Co^{2+} and Ni^{2+}), was placed at the bottom of a glass tube. This solution

was layered by a mixture of a solution of (TPrA)Br (2 mmol) in 10 ml of ethanol and a solution of Na(dca) (6 mmol) in 10 ml of water.

Single crystals of the three compounds (cubic colourless for M: Fe^{2+}, cubic pink for M: Co^{2+}, and cubic green for M: Ni^{2+}) were obtained after one week and they were collected by filtration and washed several times with ethanol.

The compounds were obtained as single phase materials and their purity was confirmed by comparison of their experimental powder X-ray diffraction (PXRD) patterns at room temperature with those simulated from the single-crystal X-ray diffraction (SCXRD) data, see Fig. S1 of ESI.†

2.2 Single-crystal X-ray diffraction

Single-crystal data sets were collected in a Bruker-Nonius x8 ApexII X-ray diffractometer equipped with a CCD detector and using monochromatic MoKα1 radiation ($\lambda = 0.71073$ Å) at different temperatures: 368 K, 323 K, 300 K (293 K in the case of the Fe compound), 200 K (180 K for the Ni compound) and 100 K. Suitable crystals of each sample were chosen and mounted on a glass fiber using instant glue. For the 100 K and 200 K (or 180 K) sets, the crystal temperature was maintained using a cold stream of nitrogen from a Kyroflex cryostream cooler. Data integration and reduction was performed using the Apex2 V.1.0 27 (Bruker-Nonius, 2005) suite software. The intensity collected was corrected for Lorentz and polarization effects, and for absorption by semi-empirical methods on the basis of symmetry-equivalent data using SADABS (2004) from the suite software. The structures were solved by the direct method using the SHELXS-97 program[20] and were refined by the full-matrix least-squares method on the SHELXL-97 program,[20] both programs are available within the WinGX package.[21] To solve the structures, anisotropic thermal factors were employed for the non-H atoms and non-disordered atoms. In the case of ordered TPrA cations, the hydrogen atoms of the propyl groups were added to the ideal positions and isotropic thermal factors were refined.

2.3 Powder X-ray diffraction

A Siemens D-5000 diffractometer using CuKα radiation ($\lambda = 1.5418$ Å) was used to study these compounds by X-ray powder diffraction (XRPD) at room temperature. The XRPD pattern was compared with the profile obtained from the single crystal structure that was generated using Mercury 3.5.1 software.[22]

2.4 Differential scanning calorimetry

Differential scanning calorimetry (DSC) studies were carried out in a TA Instruments MDSC Q2000 equipped with a liquid nitrogen cooling system. The samples (each with a mass around 5 mg) were heated and cooled with a rate of 20 K min^{-1} (2 K min^{-1} in the case of the Ni compound) from 135 to 375 K under a nitrogen atmosphere.

Additionally, pressure differential scanning calorimetry (PDSC) tests were performed in a TA Instruments pressure cell mounted on a Q2000 modulated DSC. The cell was calibrated for temperature and heat with indium at each of the pressures to be used in the measuring tests. The effect of pressure on the

melting temperature and enthalpy of indium was taken into account.[23] In a typical experiment, about 5 mg of each sample was confined inside a pinhole aluminum capsule. The experiments were performed in N_2 atmosphere at a constant pressure (from 1 to 69 bar) while keeping a constant flow of 50 ml min^{-1} of N_2. The samples under a constant external pressure were heated and cooled at a rate of 2 K min^{-1} from room temperature to 343 K.

2.5 Pressure–volume–temperature (PVT) analysis

To study the dilatometry of the materials at different pressures, PVT 100 SWO/ThermoHaake equipment was used. In a typical experiment, about 440 mg of powder material was loaded inside a cylinder between two pistons that transmit an axial compressive force from 200 to 1600 bar to the samples. After applying the external pressure, the samples were heated at a rate of 5 K min^{-1} from 183 K to 373 K and the axial thermal expansion of the samples was registered.

2.6 Dielectric measurements

The complex dielectric permittivity ($\varepsilon_r = \varepsilon_r' - i\varepsilon_r''$) of the cold-press pelletized samples were measured as a function of frequency and temperature with a parallel-plate capacitor coupled to a Solartron 1260A Impedance/Gain-Phase Analyzer, capable of measuring in the frequency range from 10 µHz to 32 MHz using an amplitude of 2 V. The capacitor was mounted in a Janis SVT200T cryostat refrigerated with liquid nitrogen, and with a Lakeshore 332 incorporated to control the temperature from 78 to 400 K. Data were collected upon heating.

Pelletized samples, made from cold-press non-oriented single crystals with an area of approximately 133 mm^2 and a thickness of approximately 1.3 mm, were prepared to fit into the capacitor, and gold was sputtered on their surfaces to ensure a good electrical contact with the electrodes.

All the dielectric measurements were carried out in a nitrogen atmosphere where several cycles of vacuum and nitrogen gas were performed to ensure that the sample environment was free of water.

Additionally, dielectric measurements were carried out in a pressure cell supplied by Novocontrol GmbH. The cell, basically a stainless steel cylinder with a hermetic seal, was filled with a silicone fluid that transmits an isostatic pressure from the piston to the sample. The dielectric response was measured for 10^3–10^6 Hz frequencies. The measurements were performed as a function of temperature (310–380 K) for constant pressures up to 2000 bar.

3. Results and discussion

3.1 Studies at ambient pressure

3.1.1 DSC results. As shown in Fig. 1, the DSC curves of the three compounds show three pairs of endothermic/exothermic peaks in the heating/cooling runs, revealing that each of them undergoes three reversible phase transitions in the temperature interval 135–375 K. The temperatures for such transitions are summarized in Table 1.
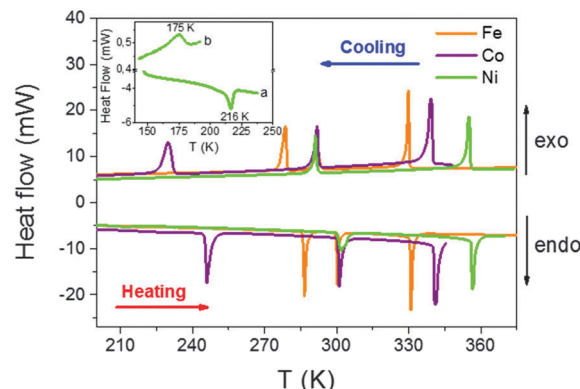

Fig. 1 DSC results as a function of temperature obtained by heating and cooling the samples (TPrA)[M(dca)$_3$] (M: Fe^{2+}, Co^{2+} and Ni^{2+}) at a rate of 20 K min^{-1}. Inset: Detail of the DSC curve for the Ni compound around T1 (a) on heating at a rate of 20 K min^{-1}, and (b) on cooling at a rate of 2 K min^{-1}.

Table 1 Summary of structural transition temperatures for Fe, Co and Ni compounds obtained from DSC analysis on heating and cooling

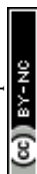|	Heating			Cooling		
	T1 (K)	T2 (K)	T3 (K)	T1 (K)	T2 (K)	T3 (K)
Fe	286	300	331	279	292	330
Co	246	301	341	230	292	339
Ni	216	302	356	175	291	355

The observed thermal hysteresis indicates the first order character of such transitions, whose associated enthalpy and entropy changes are indicated in Table S1 of the ESI.†

Taking into account that for an order–disorder transition $\Delta S = R \ln(N)$, where R is the gas constant and N is the ratio of the number of configurations in the disordered and ordered system, a value of $N \sim 1.2$–2.6 is calculated for each transition, depending also on the given compound (see Table S1 of ESI†). Such values are much lower than in the case of the analogue Mn compound, [TPrA][Mn(dca)3], that exhibits a single phase transition with $N \sim 8$.[19]

In the case of the Ni compound, we have to note that we identified, by DSC, the previously reported high temperature structural transition at $\sim$210 K.[18] Nevertheless, we were not able to also find the reported lower temperature structural transition ($\sim$160 K), not even when measuring at the slow temperature rate of 2 K min^{-1}. As we will show below,[18] this result is in agreement with our single-crystal X-ray diffraction analysis, which also does not show the previously reported re-entrant structural transition at 160 K for this compound. We attribute this lack of transition to kinetic factors.

3.1.2 Crystal structures and structural transitions as a function of temperature. In order to understand the origin of these phase transitions, the crystal structures of the Fe, Co and Ni compounds were investigated at different temperatures.

According to SCXRD, these compounds display four polymorphs (hereafter named as I, Ia, Ib and II) from 100 K to 368 K, all based on perovskite-like structures.

This journal is © The Royal Society of Chemistry 2016

J. Mater. Chem. C, 2016, 4, 4889–4898 | 4891

In the following paragraphs, we will comparatively describe the obtained structures, paying special attention to the novel polymorphs (four, in the case of the Fe and Co compounds, two in the case of the Ni compound), and focussing on details that are relevant to understand the properties.

The crystallographic data for the four polymorphs of each of the three compounds are compiled in Tables S2–S4 of the ESI,† and a summary of selected bond lengths and angles is provided in the Tables S5–S8 of the ESI.†

Polymorph I. Below 286 K (M: Fe^{2+}), 246 K (M: Co^{2+}) and 216 K (M: Ni^{2+}) the structure of these compounds is tetragonal, space group $P\bar{4}2_1c$ (non-centrosymmetric), and it can be described as a $2a \times 2a \times 2a$ perovskite super-structure.

The asymmetric unit is defined by one independent metal cation, three dca anions and three TPrA cations. The metal cations are in a distorted $[MN_6]$ octahedral environment with six different M–N distances, see Table S5 of the ESI.† The resulting $[MN_6]$ octahedra are rotated cooperatively along the main crystallographic axes (tilt systems $a^-b^+c^-$ at Glazer notation).[24] The TPrA cations are located inside the cavities of the resulting framework.

As it also occurs in the other polymorphs, and as it could be expected, as the size of the M (perovskite B-site cation) decreases from Fe^{2+} to Ni^{2+}, the unit cell volume and the M–N bond lengths were observed to decrease. In addition, the octahedra tilting in the ab plane decreases.

As seen in Fig. 2, the structures exhibit a certain disorder in the dca anions (in the *N*-amide atoms along the *c*-axis) and in the C atoms of the TPrA cations, as it was previously described for the Ni and Mn compounds.[18,19] In addition, we remark a most interesting new feature: half of the TPrA cations inside the pseudo-cubooctahedral cavities (those located on a 2-fold axis) show a cooperatively off-center shift along the *c*-axis,
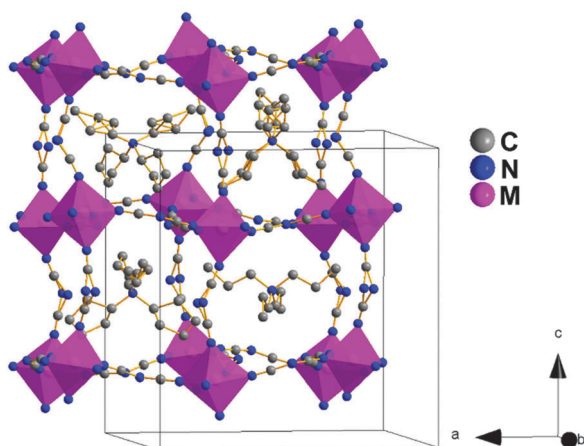
following an antiferrodistortive up-down/up-down pattern, see Fig. S2 of the ESI.†

Such displacement, that increases as the size of the M (B-site cation) decreases, is 0.095(9) Å (M: Fe^{2+}), 0.069(0) Å (M: Co^{2+}) and 0.038(2) Å (M: Ni^{2+}).

The characteristics of this low temperature polymorph are similar to those recently reported for polymorph I of the Mn analogue[19] where the TPrA shift along the *c*-axis is even larger (0.105(3) Å).

In the case of the Ni compound, for which this polymorph I has already been described before,[18] a re-entrant phase transition from polymorph I to polymorph Ia (described below) at 160 K is also reported.[18] Nevertheless, our SCXRD data (supported by our DSC analysis) do not reveal this structural transition. The polymorph I is maintained down-to 100 K. Therefore, we rationalize that the previously reported re-entrant structural transition could be related to kinetic factors that depend on the cooling rate and stabilization time.

Polymorph Ia. At T1 (see Table 1), the structure of polymorph I transforms into that of polymorph Ia of orthorhombic symmetry, space group *Pnna* (centrosymmetric) and a different $2a \times \approx 2\sqrt{2}a \times \approx 2\sqrt{2}a$ perovskite super-lattice, where $a_{pol.Ia} \approx c_{pol.I}$, and $b_{pol.Ia}$, $c_{pol.Ia} \approx \sqrt{2}a_{pol.I}$, see Tables S2–S4 of the ESI.†

The asymmetric unit contains two independent metal cations, eight dca anions and four TPrA cations. As in polymorph I, each metal cation is in a distorted octahedral environment with six different M–N distances (see Table S6 of the ESI†) and the $[MN_6]$ octahedra are cooperatively rotated following an $a^-b^+c^-$ tilt system.

On the other hand, and as could be expected, this polymorph Ia shows a slightly larger disorder than polymorph I (Fig. 3). The positions of the *N*-amide of the dca ligands along the *a*-axis had to be modeled occupying two (or three positions depending on the dca ligand) with equal occupancies; also, three of the four TPrA cations in the asymmetric unit present disorder in the C atom positions of their propyl groups.
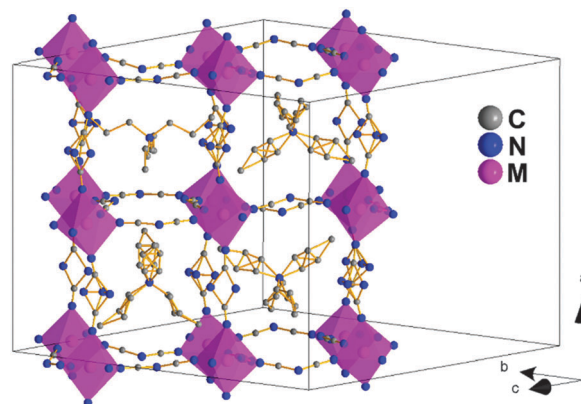

Fig. 2 Conventional perovskite structure view and unit cell of polymorph I. The dca ligands act as μ_{1-5} bridges between the M cations. The *N*-amide atom of the dca ligands along the *c*-axis are modeled in two crystallographic positions. The TPrA cations are located inside the pseudo-cubooctahedral cavities, and two of the three present in the asymmetric unit display crystallographic disorder in the C atom positions. The H-atoms of the TPrA cations have been omitted to facilitate visualization of the structure.

Fig. 3 Perovskite structure view and unit cell of polymorph Ia. The *N*-amide atom of the dca ligands along the *c*-axis show more thermal disorder than in polymorph I and they are modeled in either two or three crystallographic positions. In addition, three of the four TPrA cations in the asymmetric unit show disorder in the C atoms. The H atoms of the TPrA cations have been omitted to facilitate visualization of the structure.

4892 | *J. Mater. Chem. C*, 2016, **4**, 4889–4898

This journal is © The Royal Society of Chemistry 2016

And most remarkably, all the TPrA cations are in off-center positions following a cooperative pattern different from that shown by polymorph I, see Fig. S3 of the ESI:† (a) half of them (those located on a 2-fold axis along the *a*-axis) show a cooperative off-center shift (about 0.23 Å, ∼15% larger than in polymorph I along such a direction) along the *a*-axis towards one side of these cavities. These displaced TPrA cations are antiferro-distortively arranged along the *b*-axis, displaying an up-down-up-down pattern. (b) The other half of the TPrA cations (those located on a 2-fold axis along the *c*-axis) show an even larger cooperative off-center shift (up to 0.62 Å) along the *c*-axis towards one edge of these cavities, following an antiferro-distortive pattern.

Polymorph Ib. At T2, the structure of these $[TPrA][M(dca)_3]$, (M: Fe^{2+}, Co^{2+} and Ni^{2+}) compounds changes again: even if its symmetry remains orthorhombic, its space group changes to *Ibam* (centrosymmetric), and it has to be described on the basis of a different $\approx\sqrt{2}a \times \approx\sqrt{2}a \times 2a$ super-lattice, see Tables S2–S4 of the ESI.†

In this case, the asymmetric unit contains one independent metal cation, two dca anions and one TPrA cation. The transition metal cations are in a slightly distorted octahedral environment with three different M–N bond lengths, see Table S7 of the ESI.† And differently from polymorph I and polymorph Ia, here the $[MN_6]$ octahedra are cooperatively rotated within the *ab* plane and display an anticlockwise arrangement along the *c*-axis (tilt systems $a^0a^0c^-$ at Glazer notation).

Also, in this polymorph, the dca ligands show a much larger disorder than in the case of polymorph Ia, especially along the *c*-axis, so that the *N*-amide atom and the C atom had to be modeled occupying the 8 and 4 positions, respectively. This increase suggests a dynamic disorder along such a direction that would imply the rotation of the dca ligands around the *c*-axis axis, see Fig. 4.

As for the TPrA cations, which are also more disordered than in polymorph Ia, the most important remark is that they are located at the center of the cavities (Fig. 4). This is in contrast to the previous polymorphs. As indicated above, half (polymorph I) or all of them (polymorph Ia) are off-shifted.

Polymorph II. At T3 (see Table 1) the structure of these compounds changes again and transforms into that of polymorph II with tetragonal symmetry and space group *I4/mcm* (centrosymmetric), even if the same perovskite super-lattice as polymorph Ib, $\approx\sqrt{2}a \times \approx\sqrt{2}a \times 2a$. In fact, the space group of that lower temperature polymorph is a subgroup of polymorph II.

In that context, both polymorphs Ib and II are quite similar and their main differences rely on their symmetry and the even larger disorder of the dca ligands and TPrA cations in this higher temperature polymorph, see Fig. 5. On the other hand, and as in polymorph Ib, the TPrA cations remain centered in the cavities.

Therefore, different from the previous transitions, this occurs only at T3 and involves order/disorder phenomena with no ionic displacements.
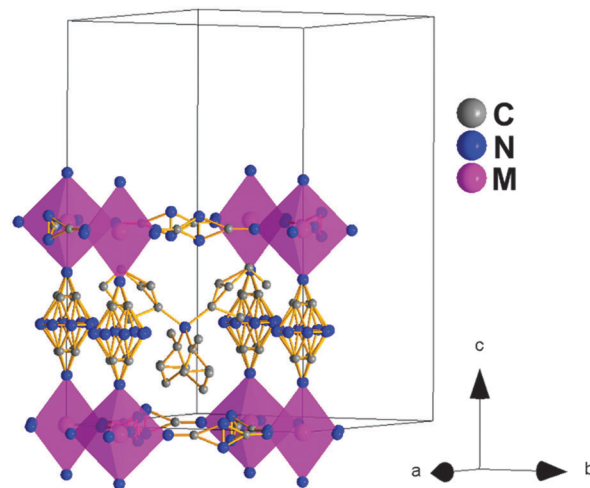

Fig. 4 Crystal structure view and unit cell of polymorph Ib. The *N*-amide and C atoms of the dca ligands along the *c*-axis are modeled in the 8 and 4 crystallographic positions, respectively. Moreover, the *N*-amide atom of the dca ligands in the *ab* plane is modeled in two crystallographic positions. As for the TPrA cations, all of them display thermal disorder in the C atoms.
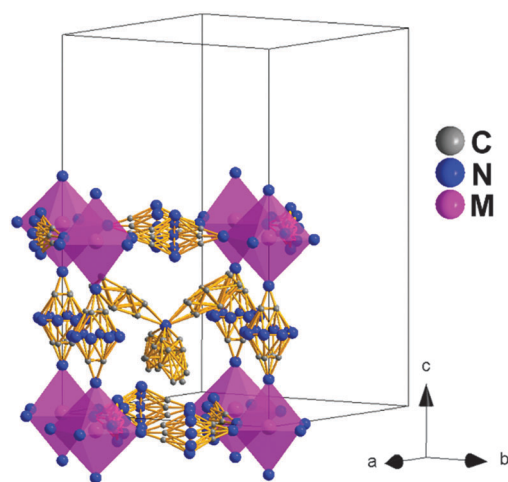

Fig. 5 Conventional perovskite structure view and unit cell of polymorph II. Similar to polymorph Ib, the *N*-amide and C atoms of the dca ligands along the *c*-axis are modeled in the 8 and 4 crystallographic positions, respectively. Meanwhile, the *N*-amide and C atoms of the dca ligands in the *ab* plane are modeled in 5 and 3 crystallographic positions, respectively. In addition, all the TPrA cations display and even higher disorder in the C atoms.

This polymorph II of the Fe, Co and Ni compounds is similar to that recently reported for the Mn compound above 330 K.[19]

3.1.3 Dielectric properties. The temperature dependence of the real part of the complex dielectric permittivity, ε_r', (also known as the dielectric constant) of $(TPrA)[M(dca)_3]$ (M: Fe^{2+}, Co^{2+} and Ni^{2+}) is shown in Fig. 6. Very interestingly, as can be seen in Fig. 6, in the three compounds, three anomalies are detected in the vicinity of the structural phase transition, those occurring at T1 and T2 being sharper than that taking place at T3, specially the first one.
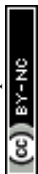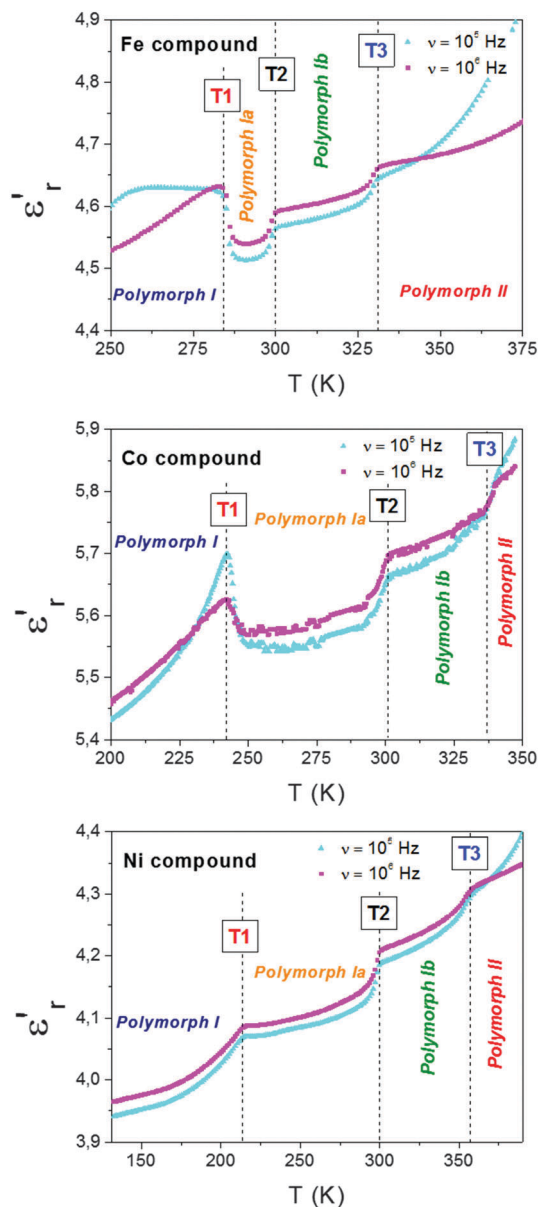
Fig. 6 Temperature dependence of the dielectric constant (ε_r') of the Fe, Co and Ni compounds measured at different frequencies (10^5–10^6 Hz).

Taking into account the previous structural information, we ascribe such anomalies to the following processes:

(a) At T1, the dca ligands remain disordered in both polymorphs mainly due to the cooperative displacement of the TPrA cations between two different antiferrodistortive arrangements that involve off-centered positions. (b) At T2, we relate it to the displacement of the TPrA cations (which are off-center shifted in polymorph Ia) to center positions in polymorph Ib. In addition, the increase disorder experienced by the polar dca ligands could also be contributing to the observed dielectric anomaly. (c) Finally, at T3, we relate it to the additional order/disorder transition experienced by both the dca ligands and TPrA cations on passing from polymorph Ib to polymorph II.

This situation is reminiscent of that recently described for the Mn analogue, where a dielectric anomaly is observed above room temperature, $T_t \sim 330$ K, associated to the change from a cooperative to a non-cooperative electric behaviour (antiferroelectric (AFE) to paraelectric (PE) transition). The former implies an AFE distribution of electric dipoles in polymorph I, related to an off-shift of the apolar TPrA cations and the order–disorder of the polar dca ligands mechanisms.

Nevertheless, in the case of here studied, (TPrA)[M(dca)$_3$] (M: Fe^{2+}, Co^{2+} and Ni^{2+}), they not only show one but multiple dielectric anomalies that are related to the richer assortment of crystal structures displayed by these compounds.

Another aspect that should be emphasized is the significant difference in the origin of the dielectric transitions displayed by these (TPrA)[M(dca)$_3$] (M: Mn^{2+}, Fe^{2+}, Co^{2+} and Ni^{2+}) compounds, and those previously reported for nother hybrid perovskites such as [AmineH][M(X)$_3$], (AmineH: midsized alkylammonium cations, X: N$_3^-$, CN$^-$ or HCOO$^-$ ligands).[8-17] These latter contain polar cations inside the cubooctahedral cavities and/or H-bonds between the cations and the framework, and their dielectric transitions arise from order–disorder processes of the guest polar molecules.

Nevertheless, in the case of this novel dicyanamide family of [TPrA][M(dca)$_3$] (M: Mn^{2+}, Fe^{2+}, Co^{2+} and Ni^{2+}), the guest TPrA cations are non-polar and cannot form H-bonds, so that the mechanisms associated with the dielectric response are completely different, namely: (a) this response is related to a contribution of a cooperative off-shift of the guest TPrA cations inside the cavities that is reminiscent of the behaviour shown by ceramic ferroelectrics with perovskite structure, such as BaTiO$_3$ (where the B-site cation is the one experiencing the temperature dependent reversible displacement, giving rise to the electric order). (b) It is also related to order–disorder processes driven by the polar dca ligands. This interesting feature can provide a novel mechanism to couple the magnetic and dielectric response of these compounds since the dca bridges are also involved in the magnetic interaction between the metal cations.

3.2 Influence of external and internal pressure on the structural and dielectric transition

In what follows, we will show that these compounds are very sensitive to both applied external pressures, even small ones ($P < 2$ kbar), as well as to internal chemical pressure induced by modifying the size of the B-site cations.

3.2.1 Influence of external pressure. We have studied the behaviour of the axial dilatometry of these samples under applied external pressures in the range $200 \leq P(\text{bar}) \leq 1600$. As it can be seen in Fig. 7, the *PVT* analysis allows an easy monitoring of the transition temperatures as a function of pressure, as a kink-shaped anomaly is observed in the curves at T1, T2 and T3.

Interestingly, the kinks at T1 and T3 are highly pressure dependent, while no significant pressure dependence is observed for that appearing at T2.

As for the kink observed at T1, that implies an increase in the axial length. It gets progressively displaced towards higher
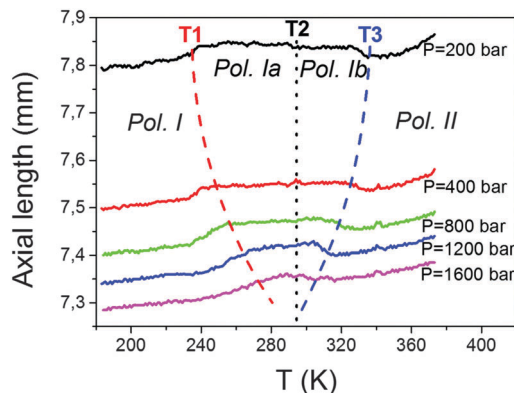
4894 | *J. Mater. Chem. C*, 2016, **4**, 4889–4898

This journal is © The Royal Society of Chemistry 2016

Fig. 7 *PVT* graphic showing the length variation of the Co sample as a function of temperature measured at different axial pressures (from 200 to 1600 bar). Dash lines signal the temperature shift of T1, T2 and T3 as a function of pressure. Similar results are obtained for the other Fe and Ni compounds.

Fig. 9 Temperature dependence of the dielectric constant (ε_r') of the Co compound, measured at 10^5 Hz under hydrostatic pressure conditions, from 1 to 2000 bar. The curves have been normalized and displaced for a better view. The Fe and Ni compounds exhibit a similar behaviour.

temperatures as pressure increases, that is, it exhibits positive pressure dependence, $\delta T_t/\delta P \approx +23$ K kbar^{-1}. This value is of the same order for the Mn compound previously reported, $\delta T_t/\delta P = +24.2$ K kbar^{-1}.[19] Meanwhile, the anomaly observed at T3, which implies a sharp decrease in the axial length, gets progressively displaced towards lower temperatures upon application of increasing pressures. This means that this transition displays a negative pressure dependence, $\delta T_t/\delta P < 0$, whose absolute value is similar to that of the previous case, even if negative, $\delta T_t/\delta P \approx -23$ K kbar^{-1}.

To further deepen the peculiar pressure dependence of the transition occurring at T3, we have performed additional pressure differential scanning calorimetry (PDSC) studies applying smaller pressures (up to 69 bar).

As can be seen in Fig. 8, both the endothermic and exothermic peaks associated with this transition experience a progressive displacement towards lower temperatures as pressure is increased, with a value of $\delta T_{t3}/\delta P = -18.4$ K kbar^{-1}, of the same order to that found in the *PVT* experiments. Meanwhile, we observed that the enthalpy (ΔH) and entropy (ΔS) changes involved in such a transition remained constant under the applied external pressure.
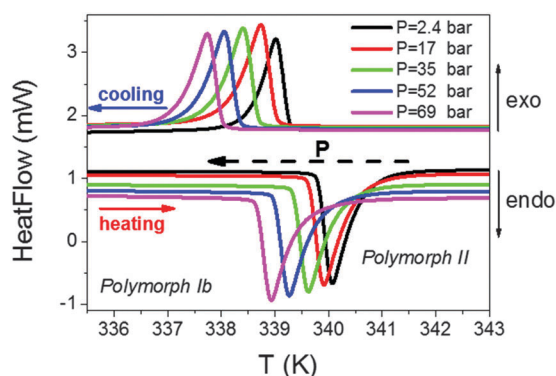

Fig. 8 Pressure differential scanning calorimetry (PDSC) curves for the T3 transition of the Co compound. Similar behaviour is found in the Fe and Ni compounds.
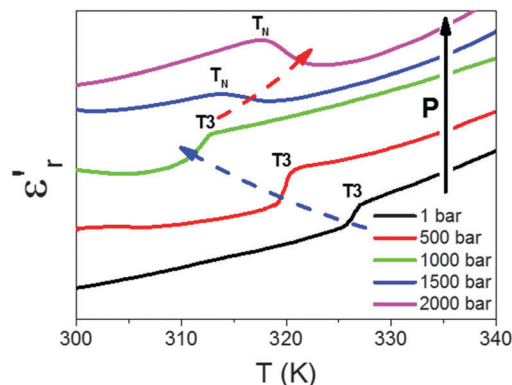
We have also studied the effect of external pressures (up to $P \leq 2000$ bar) in the temperature dependence of the dielectric permittivity of these compounds. As an example of such behaviour, we show in Fig. 9 the effect of external pressure on the dielectric response of the Co-compound in the temperature range where the anomaly at T3 is detected.

As can be seen, for $P < 1500$ bar, the kink observed at T3 in the ε_r' vs. T curve experiences a progressive displacement towards lower temperatures as pressure increases, in agreement with previous experiments.

Meanwhile, and very interestingly, when pressures that are higher than those previously used are applied, $P \geq 1500$ bar, the shape of the kink changes and a new transition (T_N) is found, which gets shifted to higher temperatures as pressure is further increased.

Taking into account that the shape and pressure dependence of such a peak is similar to that experienced by the Mn compound,[19] we ascribe it to a new pressure-induced structural transition transforming directly polymorph I to polymorph II in these Fe, Co and Ni compounds.

This in turn means that polymorphs Ia and Ib become thermodynamically unstable under applied pressure, and that both will disappear for $P > 1600$ bar. In fact, for higher pressures, a single structural transition between polymorph I and II is expected, similar to the case of the Mn analogue.[19]

3.2.2 Influence of internal chemical pressure. Chemical pressure is a well-established physical variable that can greatly affect the properties of perovskites, as widely recognized in the field of perovskite oxides ABO$_3$.[3,4,25–27]

As it is well-known in those compounds, the origin of the internal chemical pressure is in the size mismatch that occurs when the A-site ions are too small to fill the space in the three-dimensional network of the [MO$_6$] octahedral. This mismatch can be estimated as $\eta = 1 - \alpha$, which is the deviation of the tolerance factor (α) of the structure from the ideal value.[25–27]

Extending this idea to the here studied [TPrA][M(dca)$_3$] (M = Mn^{2+}, Fe^{2+}, Co^{2+} and Ni^{2+}) perovskite compounds, where the ionic radius of the B-site cations follows the sequence

This journal is © The Royal Society of Chemistry 2016

J. Mater. Chem. C, 2016, **4**, 4889–4898 | **4895**

r_B: Mn^{2+} > Fe^{2+} > Co^{2+} > Ni^{2+}, it can be expected that the tolerance factor will increase along the series while the internal pressure will decrease.

Moreover, we have calculated the value of such tolerance factors (α) following the approach recently introduced by Kieslich et al.[28] to extend the concept of Goldschmidt's tolerance factor to hybrid inorganic–organic perovskites.

For that purpose, and using the modified Goldschmidt's equation, $\alpha = (r_{A(eff)} + r_{X(eff)})/\sqrt{2}(r_B + 0.5h_{X(eff)})$,[28] we have calculated the value of α from experimental room temperature crystallographic data of A-site (TPrA) and X-site (dca) ions and using the Shannon ionic radii tables[29] for the B-site (transition metal) cations.

From the obtained values, which are summarized in Table S6 of the ESI† and range between 1.02(6) (M: Mn^{2+}) and 1.05(9) (M: Ni^{2+}), it is worth highlighting two aspects: (a) they reflect the expected increase in the tolerance factor as the size of B decreases, even if the large values of X (and A) prevent them from a larger variation. (b) Taking into account the large and complex A and X ions involved, and the simplicity of the model assumed to calculate their effective ionic sizes, the values obtained for the tolerance factor are extremely good. They fit very nicely within the TF region for which perovskite structures are expected to form (between 0.8–1.0 ± 6%)[28] even if in this particular [TPrA][M(dca)₃] system the upper limit is going to be slightly larger. These results also indicate that, in this dicyanamide series, the formation of hexagonal polytypes will require at least α > 1.05(9).

Another very interesting point that comes out from these results is the parallelism between the effect on internal pressure and external pressure on the structure of these dicyanamide compounds: both increasing external pressure or increasing the size of B reduces the temperature range in which the intermediate polymorphs Ia and Ib exist, until they finally disappear, as observed for the case of the Mn compound and for external pressures above 1500 bar, see Fig. S4 of the ESI.†

A final aspect that is worth referring to is the origin of the different pressure dependences displayed by the three consecutive temperature-induced phase transitions, and whose trend is again similar in the case of external and internal pressure. In that context, and as mentioned before, while the transition occurring at T1 shows the more commonly observed $\delta T_t/\delta P > 0$, that at T3 shows a more scarcely seen pressure dependence of the negative sign $\delta T_t/\delta P < 0$, and that at T2 is almost pressure independent.

To understand this behaviour, it is interesting to revisit previous studies carried out on oxidic and halidic perovskites, which have established that the sign of $\delta T_t/\delta P$ can depend on two factors: (a) the mechanism of the phase transition, whether it is displacive or an order–disorder type, and (b) the value of the tolerance factor that determines the change of stability of its cubic phase under P.[30]

As for (a), order–disorder transitions can be responsible for $\delta T_t/\delta P < 0$, while displacive transitions give $\delta T_t/\delta P > 0$.[30] In the case of (b), when α is below the ideal value 1, the pressure reduces the stability of the cubic phase and favours those of lower symmetry, resulting in $\delta T_t/\delta P > 0$. Meanwhile in systems with $\alpha > 1$ and hexagonal stacking, pressure stabilizes the cubic stacking at the expense of the former, resulting in $\delta T_t/\delta P < 0$.[25]

In the case of the here studied [TPrA][M(dca)₃] series, where the four compounds exhibit perovskite-like distorted structures and none of them the hexagonal stacking expected for $\alpha > 1$, we relate the different pressure dependences displayed by the three consecutive temperature-induced phase transitions to the prevailing mechanism of each of them: this would be the displacive one in the transition occurring at T1 and the order–disorder one in the case of T3. Meanwhile, the close competition between these two mechanisms in the case of T2 will result in almost no pressure dependence.

These external/internal pressure-responses reveal an easy tuning of the structural transition temperature for these hybrid perovskites. Since these structural transitions are in turn related to the dielectric properties, they can be used to modulate different dielectric responses in a wide range of temperatures near room temperature (from 210 to 360 K) either by applying small external pressures ($P < 2$ kbar) or simply by making appropriate ionic substitutions.

Therefore, this family of [TPrA][M(dca)₃] dicyanamides provides promising technological applications as dielectric transductors, sensitive towards small changes of temperature and pressure values, that can even be easily modulated by appropriate ionic substitutions.

4. Conclusions

The hybrid inorganic–organic [TPrA][M(dca)₃] (M: Fe^{2+}, Co^{2+} and Ni^{2+}) compounds are singular materials with perovskite-type structure. In these materials, [MN_6] octahedral are linked by $\mu_{1,5}$-dca bridges forming pseudo cubooctahedral cavities, that hold TPrA cations inside. Remarkably, they exhibit multiple phase transitions, that display up to three first-order structural transition between four different polymorphs (I, Ia, Ib and II) in a range of temperatures near room temperature (210–360 K). This finding is in contrast with the analogous Mn compound that only displays one first-order transition at $T_t \sim 330$ K.

Interestingly, these compounds also show multiple dielectric anomalies that are related to their richer assortment of crystal structures. Another aspect that should be emphasized is the significant difference in the origin of the dielectric transitions displayed by these (TPrA)[M(dca)₃] (M: Fe^{2+}, Co^{2+} and Ni^{2+}) compounds, and those previously reported for other hybrid perovskites. In the case of these novel dicyanamide perovskite-like compounds, the guest TPrA cations are non-polar and cannot form H-bonds, so that the mechanisms associated with the dielectric response are related to: (a) the contribution of a cooperative off-shift of the guest TPrA cations inside the cavities; and (b) order–disorder processes driven by the polar dca ligands.

In addition, we have studied the parallelism between the effect of the external hydrostatic pressure ($P < 2$ kbar) and the internal chemical pressure (by modifying the ionic radii and thereby the tolerance factor) on the phase and dielectric transitions.

4896 | J. Mater. Chem. C, 2016, 4, 4889–4898

This journal is © The Royal Society of Chemistry 2016

It is important to highlight that we can modulate the structural and dielectric transition temperature as a function of external/internal pressure: by increasing the external pressure or increasing the M (perovskite B-site cations) ionic radii (decreasing the tolerance factor), we can reduce the thermal stability of the intermediate polymorphs Ia and Ib, and even suppress them.

Therefore, the hybrid perovskites [TPrA][M(dca)$_3$] (M: Fe^{2+}, Co^{2+} and Ni^{2+}) are unique multi-sensitive materials where their multiple phase and dielectric transitions can be easily tuned as a function of external pressures as well as by internal chemical pressure. To our knowledge, these are the first examples of hybrid inorganic–organic perovskite-like materials with multiple dielectric transitions that offer easy temperature, pressure and chemical modulation. In that event, these singular materials offer potential interest for future technological applications such as temperature and pressure sensing.

Acknowledgements

Notes and references

1 (a) P. Granger, V. I. Parvulescu, S. Kaliaguine and W. Prellier, *Perovskites and Related Mixed Oxides: Concepts and Applications*, Wiley-VCH, Weinheim, Germany, 2015; (b) F. S. Galasso, *Structure, properties, and preparation of perovskite-type compounds*, Pergamon Press, New York, 1969; (c) M. A. Peña and J. L. G. Fierro, *Chem. Rev.*, 2001, **101**, 1981–2018.

2 (a) M. E. Lines and A. M. Glass, *Principles applications of ferroelectric and related materials*, Oxford Unviersity Press, New York, 2001; (b) F. Jona and G. Shirane, *Ferroelectric Crystals*, Pergamon Press, Oxford, 1962.

3 J. M. Tarascon and B. G. Bagley, in *Chemistry of super-conducting materials*, ed. T. A. Vanderah, Noyes Publications, 1992.

4 C. N. R. Rao and B. Raveau, *Colossal magnetoresistance, charge ordering and related properties of Manganese oxides*, World Scientific Publications, Hackensack, NJ, USA, 2004.

5 N. A. Spaldin and M. Fiebig, *Science*, 2005, **309**, 391–392.

6 D. Mitzi, in *Prog. Inorg. Chem.*, ed. K. D. Karlin, John Wiley & Sons, New York, USA, 1999, ch. 1, vol. 48.

7 (a) M. M. Lee, J. Teuscher, T. Miyasaka, T. N. Murakami and H. J. Snaith, *Science*, 2012, **338**, 643–647; (b) J. Burschka, N. Pellet, S. J. Moon, R. Humphry-Baker, P. Gao, M. K. Nazeeruddin and M. Grätzel, *Nature*, 2013, **499**, 316–319; (c) N. J. Jeon, J. H. Noh, W. S. Yang, Y. C. Kim, S. Ryu, J. Seo and S. I. Seok, *Nature*, 2015, **517**, 476–480; (d) M. Sessolo and H. J. Bolink, *Science*, 2016, **350**, 917.

8 (a) X.-H. Zhao, X.-C. Huang, S.-L. Zhang, D. Shao, H.-Y. Wei and X.-Y. Wang, *J. Am. Chem. Soc.*, 2013, **135**, 16006–16009; (b) Z.-Y. Du, Y.-P. Zhao, W.-X. Zhang, H.-L. Zhou, C.-T. He, W. Xue, B.-Y. Wang and X.-M. Chen, *Chem. Commun.*, 2014, **50**, 1989–1991; (c) Z.-Y. Du, Y.-P. Zhao, C.-T. He, B.-Y. Wang, W. Xue, H.-L. Zhou, J. Bai, B. Huang, W.-X. Zhang and X.-M. Chen, *Cryst. Growth Des.*, 2014, **14**, 3903–3909; (d) Z.-Y. Du, Y.-Z. Sun, S.-L. Chen, B. Huang, Y.-J. Su, T.-T. Xu, W.-X. Zhang and X.-M. Chen, *Chem. Commun.*, 2015, **51**, 15641–15644; (e) Z.-Y. Du, T.-T. Xu, B. Huang, Y.-J. Su, W. Xue, C.-T. He, W.-X. Zhang and X.-M. Chen, *Angew. Chem.*, 2015, **127**, 928–932; (f) L. C. Gómez-Aguirre, B. Pato-Doldán, A. Stroppa, L.-M. Yang, T. Frauenheim, J. Mira, S. Yáñez-Vilar, R. Artiaga, S. Castro-García, M. Sánchez-Andújar and M. A. Señarís-Rodríguez, *Chem. – Eur. J.*, 2016, DOI: 10.1002/chem.201503445.

9 (a) W. Zhang, Y. Cai, R.-G. Xiong, H. Yoshikawa and K. Awaga, *Angew. Chem., Int. Ed.*, 2010, **122**, 6758–6760; (b) W. Zhang, H.-Y. Ye, R. Graf, H. W. Spiess, Y.-F. Yao, R.-Q. Zhu and R.-G. Xiong, *J. Am. Chem. Soc.*, 2013, **135**, 5230–5233; (c) X. Zhang, X.-D. Shao, S.-C. Li, Y. Cai, Y.-F. Yao, R.-G. Xiong and W. Zhang, *Chem. Commun.*, 2015, **51**, 4568–4571; (d) W.-J. Xu, S.-L. Chen, Z.-T. Hu, R.-B. Lin, Y.-J. Su, W.-X. Zhang and X.-M. Chen, *Dalton Trans.*, 2016, **45**, 4224–4229.

10 (a) P. Jain, N. S. Dalal, B. H. Toby, H. W. Kroto and A. K. Cheetham, *J. Am. Chem. Soc.*, 2008, **130**, 10450–10451; (b) P. Jain, V. Ramachandran, R. J. Clark, H. D. Zhou, B. H. Toby, N. S. Dalal, H. W. Kroto and A. K. Cheetham, *J. Am. Chem. Soc.*, 2009, **131**, 13625–13627; (c) Z. Zhang, W. Li, M. A. Carpenter, C. J. Howard and A. K. Cheetham, *CrystEngComm*, 2015, **17**, 370–374; (d) G. Kieslich, A. C. Forse, S. Sun, K. T. Butler, S. Kumagai, Y. Wu, M. R. Warren, A. Walsh, C. P. Grey and A. K. Cheetham, *Chem. Mater.*, 2016, **28**, 312–317; (e) G. Kieslich, S. Kumagai, K. T. Butler, T. Okamura, C. H. Hendon, S. Sun, M. Yamashita, A. Walsh and A. K. Cheetham, *Chem. Commun.*, 2015, **51**, 15538–15541.

11 (a) R. Shang, G.-C. Xu, Z.-M. Wang and S. Gao, *Chem. – Eur. J.*, 2014, **20**, 1146–1158; (b) S. Chen, R. Shang, K.-L. Hu, Z.-M. Wang and S. Gao, *Inorg. Chem. Front.*, 2014, **1**, 83–98; (c) S. Chen, R. Shang, B.-W. Wang, Z.-M. Wang and S. Gao, *Angew. Chem.*, 2015, **127**, 11245–11248; (d) R. Shang, S. Chen, B.-W. Wang, Z.-M. Wang and S. Gao, *Angew. Chem.*, 2016, **128**, 2137–2140.

12 (a) M. Sánchez-Andújar, S. Presedo, S. Yáñez-Vilar, S. Castro-García, J. Shamir and M. A. Señarís-Rodríguez, *Inorg. Chem.*, 2010, **49**, 1510–1516; (b) B. Pato-Doldán, M. Sánchez-Andújar, L. C. Gómez-Aguirre, S. Yáñez-Vilar, J. López-Beceiro, C. Gracia-Fernández, A. A. Haghighirad, F. Ritter, S. Castro-García and M. A. Señarís-Rodríguez, *Phys. Chem. Chem. Phys.*, 2012, **14**, 8498–8501; (c) J. López-Beceiro, C. Gracia-Fernández, S. Gómez-Barreiro, S. Castro-García, M. Sánchez-Andújar and R. Artiaga, *J. Phys. Chem. C*, 2012, **116**, 1219–1224; (d) B. Pato-Doldán, L. C. Gómez-Aguirre, J. M. Bermúdez-García, M. Sánchez-Andújar, A. Fondado, J. Mira, S. Castro-García and M. A. Señarís-Rodríguez, *RSC Adv.*, 2013, **3**, 22404–22411; (e) M. Sánchez-Andújar,

L. C. Gómez-Aguirre, B. Pato-Doldán, S. Yáñez-Vilar, R. Artiaga, A. L. Llamas-Saiz, R. S. Manna, F. Schnelle, M. Lang, F. Ritter, A. A. Haghighirad and M. A. Señarís-Rodríguez, *CrystEngComm*, 2014, **16**, 3558–3566; (*f*) L. C. Gómez-Aguirre, B. Pato-Doldán, A. Stroppa, S. Yáñez-Vilar, L. Bayarjargal, B. Winkler, S. Castro-García, J. Mira, M. Sánchez-Andújar and M. A. Señarís-Rodríguez, *Inorg. Chem.*, 2015, **54**, 2109–2116.

13 (*a*) B. Zhou, Y. Imai, A. Kobayashi, Z.-M. Wang and H. Kobayashi, *Angew. Chem., Int. Ed. Engl.*, 2011, **50**, 11441–11445; (*b*) Y. Imai, B. Zhou, Y. Ito, H. Fijimori, A. Kobayashi, Z. M. Wang and H. Kobayashi, *Chem. – Asian J.*, 2012, **7**, 2786–2790.

14 (*a*) A. Stroppa, P. Barone, P. Jain, J. M. Perez-Mato and S. Picozzi, *Adv. Mater.*, 2013, **25**, 2284–2290; (*b*) Y. Tian, A. Stroppa, Y.-S. Chai, P. Barone, M. Perez-Mato, S. Picozzi and Y. Sun, *Phys. Status Solidi RRL*, 2015, **9**, 62–67; (*c*) M. Ptak, M. Mczka, A. Ggor, A. Sieradzki, A. Stroppa, D. Di Sante, J. M. Perez-Mato and L. Macalik, *Dalton Trans.*, 2016, **45**, 2574–2583.

15 (*a*) M. Mczka, A. Ciupa, A. Ggor, A. Sieradzki, A. Pikul, B. Macalik and M. Drozd, *Inorg. Chem.*, 2014, **53**, 5260–5268; (*b*) M. Mczka, A. Pietraszko, B. Macalik and K. Hermanowicz, *Inorg. Chem.*, 2014, **53**, 787–794; (*c*) M. Mczka, A. Ggor, B. Macalik, A. Pikul, M. Ptak and J. Hanuza, *Inorg. Chem.*, 2014, **53**, 457–467; (*d*) M. Mczka, A. Ggor, K. Hermanowicz, A. Sieradzki, L. Macalik and A. Pikul, *J. Solid State Chem.*, 2016, **237**, 150–158.

16 (*a*) Y. Tian, A. Stroppa, Y. Chai, L. Yan, S. Wang, P. Barone, S. Picozzi and Y. Sun, *Sci. Rep.*, 2014, **4**, 6062; (*b*) Y. Tian, S. Shen, J. Cong, L. Yan, S. Wang and Y. Sun, *J. Am. Chem. Soc.*, 2016, **138**, 782–785.

17 L. C. Gómez-Aguirre, B. Pato-Doldán, J. Mira, S. Castro-García, M. A. Señarís-Rodríguez, M. Sánchez-Andújar, J. Singleton and V. S. Zapf, *J. Am. Chem. Soc.*, 2016, **138**, 1122–1125.

18 J. A. Schlueter, J. L. Manson and U. Geiser, *Inorg. Chem.*, 2005, **44**, 3194–3202.

19 J. M. Bermúdez-García, M. Sánchez-Andújar, S. Yáñez-Vilar, S. Castro-García, R. Artiaga, J. López-Beceiro, L. Botana, A. Alegría and M. A. Señarís-Rodríguez, *Inorg. Chem.*, 2015, **54**, 11680–11687.

20 G. M. Sheldrick, *Acta Crystallogr., Sect. A: Cryst. Phys., Diffr., Theor. Gen. Crystallogr.*, 2008, **64**, 112–122.

21 L. J. Farrugia, *Appl. Crystallogr.*, 2012, **45**, 849–854.

22 Mercury 3.5.1 (Build RC5) – Crystal Structure Visualisation (CCDC) http://www.ccdc.cam.ac.uk/mercury.

23 (*a*) J. D. Dudley and H. T. Hall, *Phys. Rev.*, 1960, **118**, 1211–1216; (*b*) G. W. H. Höhne, W. Dollhopf, K. Blankenhorn and P. U. Mayr, *Thermochim. Acta*, 1996, **273**, 17–24.

24 A. M. Glazer, *Acta Crystallogr., Sect. B: Struct. Sci.*, 1972, **28**, 3384–3392.

25 J. B. Goodenough, J. A. Kafalas and J. M. Longo, in *Preparative methods in Solid State Chemistry*, ed. P. Hagenmüller, Academic press, New York, USA, 1972, ch. 1.

26 K. I. Kugel, A. L. Rakhmanov, A. O. Sboychakov, N. Poccia and A. Bianconi, *Phys. Rev. B: Condens. Matter Mater. Phys.*, 2008, **78**, 165124.

27 H. Y. Hwang, T. T. Palstra, S.-W. Cheong and B. Batlogg, *Phys. Rev. B: Condens. Matter Mater. Phys.*, 1995, **52**, 15046–15049.

28 (*a*) G. Kieslich, S. Suna and A. K. Cheetham, *Chem. Sci.*, 2014, **5**, 4712–4715; (*b*) G. Kieslich, S. Suna and A. K. Cheetham, *Chem. Sci.*, 2015, **6**, 3430–3433.

29 R. D. Shannon, *Acta Crystallogr., Sect. A: Found. Crystallogr.*, 1976, **32**, 751.

30 K. S. Aleksandrov, J. Bartolome, M. V. Gorev and I. N. Flerov, *Phys. Status Solidi B*, 2000, **217**, 785–791.